Magnetic field effects on quantum ring excitons

Jakyoung Song[1,2] and Sergio E. Ulloa[2,3]

[1]*National CRI Center for Nano Particle Control, School of Mechanical and Aerospace Engineering, Seoul National University, Seoul 151-742, Korea*

[2]*Department of Physics and Astronomy and Condensed Matter and Surface Sciences Program, Ohio University, Athens, Ohio 45701–2979*

[3]*Sektion Physik, Ludwig-Maximilians-Universität, Geschwister-Scholl-Platz 1, 80539, Germany*

We study the effect of magnetic field and geometric confinement on excitons confined to a quantum ring. We use analytical matrix elements of the Coulomb interaction and diagonalize numerically the effective-mass Hamiltonian of the problem. To explore the role of different boundary conditions, we investigate the quantum ring structure with a parabolic confinement potential, which allows the wave functions to be expressed in terms of center of mass and relative degrees of freedom of the exciton. On the other hand, wave functions expressed in terms of Bessel functions for electron and hole are used for a hard-wall confinement potential. The binding energy and electron–hole separation of the exciton are calculated as function of the width of the ring and the strength of an external magnetic field. The linear optical susceptibility as a function of magnetic fields is also discussed. We explore the Coulomb electron–hole correlation and magnetic confinement for several ring width and size combinations. The Aharanov–Bohm oscillations of exciton characteristics predicted for one-dimensional rings are found to not be present in these finite-width systems.

　　　　PACS number(s): 71.35.Ji, 71.35.Cc, 78.55.−m

I. INTRODUCTION

The fabrication of nanometer-size semiconductor structures by different techniques (including lithography, etching, direct chemical synthesis, and self-assembly, to name a few) has allowed a veritable explosion of activity in this area.[1] It is now well-known that carrier confinement into dimensions of a few tens of nanometers provides strong blueshift of the photoluminescence features from that in the original bulk material, a clear consequence of quantum confinement in these *quantum dots*. Currently, researchers are investigating a variety of magnetocapacitance and optical properties of dots,[1] including the role of inelastic light scattering and phonon confinement,[2,3] as well as Pauli blocking and other few- and many-particle effects in these systems.[4]

In recent work, however, a new geometry of semiconductor quantum *rings* has been introduced in experiments of magnetocapacitance and infrared excitation for few electrons.[5,6] Although *metallic* rings have been the subject of considerable attention for a number of years,[7] this geometry had not been achieved in semiconductors for sizes such that the electrons would propagate coherently (non-diffusively) throughout the ring. However, the self-assembled quantum rings now achieved are so small (with characteristic inner/outer radius of 20/100 nm and 2–3 nm in height), that they allow the study of a non-simply-connected geometry where carriers are coherent all throughout. It is clear that not only the single-particle states are interesting in this geometry (especially their behavior under magnetic flux), but also the role of interactions between particles (be it electrons or holes). Lorke *et al.* have shown that multiple-electron states in this geometry experience phase coherent effects in the presence of magnetic fields,[5] much as predicted by theory.[8] The question of the observability of similar coherent effects for elec-

trons *and* holes around the loop, in the presence of a magnetic field, is fascinating, and some theoretical works have already begun to explore this regime.[9–12] Although beautiful experiments of optical emission in charge-tunable quantum rings have been recently presented,[13,14] they study the role of multiply charged exciton complexes with no applied magnetic field.

The multiply connected geometry of the semiconductor quantum rings adds an interesting dimension to the strong Coulomb effects in magnetic fields which have been explored in quantum confined systems. Excitons in magnetic fields have been investigated in structures such as quantum wells,[15,16] quantum wires,[17] and quantum dots,[18–22] as examples of multicarrier systems. For the ring geometry, one question that arises naturally is whether there is sensitivity of the exciton properties to an applied flux. This ''Aharanov–Bohm effect'' (ABE) for an exciton is an interesting concept, since one would naturally associate the existence of the ABE with a net charge (as the coupling constant to the vector potential), and the net charge of this object is clearly zero. However, one could argue that the composite nature of the excitons would perhaps allow for a non-vanishing effect. In fact, for the case of particles constrained to move along a one-dimensional ring, rigorous derivations predict a non-zero ABE for the exciton, which will show in its various energy states and the associated dipole oscillator strength, for small enough rings.[10,11]

In this work, we present calculations of the excitation spectrum and oscillator strength of excitons in rings pierced by magnetic fields. We explore the role of different confinement potentials and calculate binding energies, exciton sizes, and their dependence on magnetic fields, as well as oscillator strengths which would be measurable in photoluminescence experiments, for example. Similar to the case of quantum

dots, we find strong orbital effects from the magnetic field, which provides for effectively stronger confinement and accompanying diamagnetic level shifts, as well as splitting of some levels. These changes are found to be monotonic with field. Part of our motivation in this study is to explore the question of how robust is the ABE predicted in one-dimensional (1D) rings, when one considers finite width and confinement potentials. The models we use are designed to mimic the situation in real semiconductor quantum rings achieved to date. Much to our chagrin, we find no trace of the predicted ABE for realistic values of the rings and fields in the problem. Although this negative result would suggest that it is difficult that experiments would measure this effect, it is still open to see to what extent highly sensitive experiments might be able to yield a positive result.

The remainder of this paper is organized as follows. In Sec. II, we present the model for the system and solution method. As a first approximation, the quantum ring structure is modeled by a parabolic confinement potential, in which the wave functions expressed in terms of the center of mass and relative coordinates are used as a basis set. This confinement potential has been experimentally confirmed by the recent experiments of Lorke *et al.*[5] In order to explore the role of different potentials, we also model the ring system with a hard-wall confinement, using wave functions expressed in terms of Bessel functions for electron and hole as a basis set. In Sec. III, we discuss the main effects of the magnetic field effects on the exciton characteristics, including the binding energy, electron–hole separation, and the linear optical susceptibility. Finally, we summarize our results in Sec. IV. The Appendix contains an outline of the derivation of the Coulomb matrix element with these basis functions. The analytical expressions presented there greatly simplify our calculations.

II. THEORETICAL MODEL

Our model is a two-dimensional (2D) exciton in a quantum ring and in a static magnetic field, simulating recent experimental quantum ring structures. The presence of magnetic fields oriented along the z axis, perpendicular to the plane of the ring, induces the electron and hole to perform classical orbits along the circumference, which of course yield quantization of the angular momentum in that direction.[10,11] The ring structures are well approximated by using parabolic potentials, giving soft confinement barriers, appropriate to samples produced by self-assembly.[5] For narrow rings (with steep confinement), however, the parabolic confinement and associated wave functions fail in a real system, as the increased confinement may push the levels into the anharmonic part of the potential, and even produce deconfinement of one carrier (typically the electron), as found in some calculations in quantum dots.[23] We also consider the case of hard-wall confinement and analyze the different results.

As the quantum rings and excitonic states under consideration are much larger than the unit cell of the material, the effective-mass approximation is a suitable approach, and is given by $H = H_e + H_h + H_{e-h}$, where the subscripts e and h represent electron and hole, and the last term is the electron–hole interaction. The expression for the Hamiltonian of the electron in magnetic fields (in a parabolic-band approximation) is given by

$$H_e = \frac{1}{2m_e}\left[\mathbf{p}_e + \frac{q_e}{c}\mathbf{A}_e\right]^2 + V_e, \qquad (1)$$

with a similar expression for the Hamiltonian of the hole. Here, V_e (or V_h) is the ring confinement potential for electron (hole), and naturally $q_e = -|e|$ and $q_h = +|e|$. For parabolic confinement potential across the width of the ring, we use

$$V_i = \tfrac{1}{2}m_i\omega_i^2(r_i - r_0)^2, \qquad (2)$$

where the mean radius of the ring is r_0, and the characteristic confinement energy is $\hbar\omega_i$, giving a characteristic ring width $\approx 2\sqrt{\hbar/m_i\omega_i}$ for each particle. Here, $i = e, h$ represents the different particles. We choose the fully symmetric gauge vector potentials $\mathbf{A}_e = \tfrac{1}{2}\mathbf{B}\times(\mathbf{r}_e - \mathbf{r}_h)$ and $\mathbf{A}_h = \tfrac{1}{2}\mathbf{B}\times(\mathbf{r}_h - \mathbf{r}_e)$, for electron and hole, respectively, following Refs. 18 and 21. The Coulomb interaction term between carriers is given by $H_{e-h} = -e^2/\epsilon r_{e-h}$, screened by the background dielectric constant ϵ.

A. Parabolic confinement potential

For the parabolic confinement potential it is convenient to separate the problem into center of mass and relative coordinates, described as usual by $\mathbf{r} = \mathbf{r}_e - \mathbf{r}_h$, and $\mathbf{R} = (m_e\mathbf{r}_e + m_h\mathbf{r}_h)/M$, where the total and reduced masses are $M = m_e + m_h$, and $\mu = m_e m_h/M$. The total Hamiltonian can then be re-expressed as $H = H_{CM} + H_{rel} + H_{mix}$, with individual terms

$$H_{CM} = \frac{1}{2M}P^2 + \frac{1}{2}M\omega_0^2(R - r_o)^2, \qquad (3)$$

$$H_{rel}^o = \frac{1}{2\mu}p^2 + \frac{1}{2}\mu\omega^2 r^2, \qquad (4)$$

and $H_{rel} = H_{rel}^o + H_{rel}'$, where

$$H_{rel}' = -\omega_c\gamma L_z - \frac{e^2}{\epsilon r}, \qquad (5)$$

and

$$\begin{aligned}
H_{mix} = {} & -\frac{e}{Mc}(\mathbf{B}\times\mathbf{r})\cdot\mathbf{P} - m_e\omega_0^2 r_0 \\
& \times R\left(1 + \frac{2m_h}{MR^2}\mathbf{R}\cdot\mathbf{r} + \frac{m_h^2}{M^2}\frac{r^2}{R^2}\right)^{1/2} - m_h\omega_0^2 r_0 \\
& \times R\left(1 - \frac{2m_e}{MR^2}\mathbf{R}\cdot\mathbf{r} + \frac{m_e^2}{M^2}\frac{r^2}{R^2}\right)^{1/2}, \qquad (6)
\end{aligned}$$

where $\gamma = (m_h - m_e)/M$ depends on the mass asymmetry of the carriers, and we have set $\omega_e = \omega_h = \omega_0$. We have also denoted the relative angular momentum in the z direction as $L_z = (\mathbf{r} \times \mathbf{p})_z$, and the effective confinement frequency as $\omega^2 = \omega_0^2 + \omega_c^2$, with $\omega_c = eB/(2\mu c)$, resulting from the combined confinement of the potential and the magnetic field.

The main purpose in the change of the above-mentioned variables is to use the solutions of H_{CM} and H_{rel}^o as a basis for the solution of the full Hamiltonian. The center of mass basis is essentially a harmonic oscillator, with wave function $\psi_{N,l_{CM}}$ centered about r_0,

$$\psi_{N,l_{CM}}(R) = \alpha \sqrt{\frac{2N!}{(N+|l_{CM}|)!}} \frac{1}{\sqrt{2\pi}} e^{il_{CM}\theta} e^{-\alpha^2(R-r_0)^2/2}$$
$$\times [\alpha(R-r_0)]^{|l_{CM}|} L_N^{|l_{CM}|}[\alpha^2(R-r_0)^2], \quad (7)$$

with $\alpha = \sqrt{M\omega_0/\hbar}$, and eigenvalues $E_{CM}^0 = (2N+1 +|l_{CM}|)\hbar\omega_0$. Here, N and l_{CM} are quantum numbers of the radial and angular momentum part, respectively, for the center of mass coordinates, and $L_N^{|l_{CM}|}$ is the associated Laguerre polynomial.[24] Similarly, the eigenvalues and eigenfunctions for the *non-interacting* relative Hamiltonian are given by wave function $\phi_{n,l}$ and energy E_{rel}^0, where

$$\phi_{n,l}(r) = \beta \sqrt{\frac{2n!}{(n+|l|)!}} \frac{1}{\sqrt{2\pi}} e^{il\varphi} e^{-\beta^2 r^2/2} (\beta r)^{|l|} L_n^{|l|}(\beta^2 r^2),$$
$$(8)$$

$$E_{rel}^0 = (2n+1+|l|)\hbar\omega,$$

with $\beta = \sqrt{\mu\omega/\hbar}$. Here, n and l are quantum numbers of the radial and angular momentum parts, respectively, for the relative coordinates. With this harmonic basis set, matrix elements for the Coulomb interaction, magnetic field dependent and mixing terms can be calculated analytically.[20,21] These expressions are collected in the Appendix.

The total Hamiltonian given previously is then diagonalized numerically, leading to the eigenvalues and eigenfunctions. All the physical properties of the exciton in the ring can in principle be extracted from these eigenvalues and eigenfunctions. Here, we present the binding energy, electron–hole separation, and the linear optical susceptibility of the quantum ring. These quantities are readily accessible in optical experiments of photoluminescence (PL) and photoluminescence excitation (PLE). Denoting the wave functions of the exciton as $|\Psi\rangle = \Sigma_{Nl_{CM}nl} a_{Nl_{CM}nl} |N,l_{CM},n,l,\rangle$ with coefficients $a_{Nl_{CM}nl}$ obtained from the diagonalization, one can write for example an expression for the electron–hole separation,

$$r_s^2 = \langle\Psi|r^2|\Psi\rangle$$

$$= \delta_{N',N}\delta_{l'_{CM},l_{CM}}\delta_{l',l} \sum_{Nl_{CM}nlN'l'_{CM}n'l'} a_{N'l'_{CM}n'l'}^* a_{Nl_{CM}nl}$$

$$\times \sqrt{\frac{n!n'!}{(n+|l|)!(n'+|l'|)!}} \sum_{k=0}^{n} \sum_{j=0}^{n'} \frac{(n+|l|)!(n'+|l'|)!}{(k+|l|)!(j+|l'|)!}$$

$$\times (-1)^{k+j} \frac{1}{k!(n-k)!j!(n'-j)!} \frac{1}{\beta^2}(|l|+k+j+1)!.$$
$$(9)$$

Similarly, the linear optical susceptibility is given by $\chi(\omega) = \Sigma_j |\langle 0|P|1\rangle_j|^2 (\hbar\omega - E_j - i\hbar\Gamma)^{-1}$, where $\langle 0|P|1\rangle_j$ is the dipole matrix element between one electron–hole pair j state and the vacuum state. These are proportional to the bulk interband matrix elements, p_{cv}, and can be written in terms of the envelope function as,[25]

$$|\langle 0|P|1\rangle|^2 = |p_{cv}|^2 \left| \int \Psi(\mathbf{r}_e,\mathbf{r}_h = \mathbf{r}_e) d\mathbf{r}_e \right|^2$$

$$= |p_{cv}|^2 \left\{ \delta_{l,0} \sum_n a_n \sqrt{\frac{\mu\omega}{\pi\hbar}} \right\}^2$$

$$\times \left\{ \delta_{l_{CM},0} \sqrt{2\pi} \sqrt{\frac{2N!}{(N+|l_{CM}|)!}} (-1)^N \frac{1}{\alpha} \right\}^2.$$
$$(10)$$

B. A hard-wall confinement potential

Given that the two-dimensional free exciton size (effective Bohr radius) in InAs is $a_B^{2D} \approx 16$ nm (6 nm for GaAs), the quantum rings with widths larger than $2a_B^{2D}$ would tend to yield highly symmetric (nearly circular) ground states of the exciton, with the confinement potential being a small perturbation. For narrower quantum rings, however, the symmetry of the exciton in the ring would be strongly affected, and become increasingly one dimensional. This would be favorable for the appearance of the ABE, as predicted by theory.[10,11] To allow for this different case, and so as to test the possible bias of the numerical calculations in the parabolic potential, we have also implemented solutions of the problem in a hard-wall confinement potential basis.

In that situation, the basis set for the exciton problem is given by products of the radial and angular parts of electron and hole, $\Psi = \Psi_e(r_e,\phi_e)\Psi_h(r_h,\phi_h)$, where the individual wave functions are given by (in the absence of magnetic field)

$$\Psi(r_i,\phi_i) = \psi_i(r_i) \frac{1}{\sqrt{2\pi}} e^{il_i\phi_i}, \quad (11)$$

where $i = e, h$, and l_i is an integer. The wave functions of the radial part must satisfy the hard-wall boundary conditions and vanish at both the inner (a) and outer radius ($a + 2L$) of the ring structure. As such, they are given by linear combinations of Bessel functions, $\psi_i(r_i) = A J_{l_i}(k_i r_i) + B N_{l_i}(k_i r_i)$, for $a \leqslant r_i \leqslant a + 2L$. Here, A and B are normalized constants, and J_{l_i} and N_{l_i} are the l_ith-order Bessel function of the first and second kind, respectively, with $k_i = \sqrt{2 m_i E_i / \hbar^2}$. The eigenvalue conditions are obtained from the secular equation $J_{l_e}(k_e a) N_{l_e}[k_e(a + 2L)] = N_{l_e}(k_e a) J_{l_e}[k_e(a + 2L)]$, with a similar expression for the hole states. These expressions yield the basis for the electron–hole pair problem without Coulomb interaction or magnetic field, with eigenvalues $E_0 = \hbar^2 k_e^2 / 2 m_e + \hbar^2 k_h^2 / 2 m_h$. One can conveniently write the Coulomb interaction potential matrix elements using this noninteracting pair basis via Fourier transform integrals, as done in Ref. 8 (see the Appendix).

Similarly, one can obtain the matrix elements of the Hamiltonian which depend on magnetic fields,

$$H_B = -\frac{e}{2 m_e c} \mathbf{p}_e \cdot \mathbf{B} \times \mathbf{r}_e + \frac{e^2 B^2}{8 m_e c^2} r_e^2 + \frac{e}{2 m_h c} \mathbf{p}_h \cdot \mathbf{B} \times \mathbf{r}_h$$

$$+ \frac{e^2 B^2}{8 m_h c^2} r_h^2, \tag{12}$$

by using straightforward finite domain integrals of the above-given basis set. The energies and eigenfunctions for the exciton are calculated by numerical diagonalization of the total Hamiltonian *with* magnetic fields obtained from the summation of all the above-mentioned terms. The wave functions are then represented as $|\Psi\rangle = \sum_{n_e n_h l_e l_h} a_{n_e n_h l_e l_h} | n_e, n_h, l_e, l_h \rangle$, where $a_{n_e n_h l_e l_h}$ are the coefficients calculated from the diagonalization. In turn, the mean electron–hole separation r_s and the linear optical susceptibility can be calculated.

III. RESULTS

We present here characteristic results of our calculations. As mentioned before, they are scalable for different materials, in terms of the Bohr radius of the exciton and its relation to the size (specially the width) of the ring. The parameters employed here describe GaAs, yielding an effective 2D Bohr radius of 6 nm. Figure 1 compares the exciton binding energies obtained for parabolic confinement (triangles) with those for a hard-wall confinement (diamonds), as function of the quantum ring width. Notice that $E_b = E_{e-h}^0 - E_{grnd}^{exciton}$, where the first term is only the confinement ground state of the electron and hole, ignoring the Coulomb interaction. For relatively narrow rings, the exciton binding energy for the parabolic confinement model is much larger than for the hard-wall confinement, as expected. This difference is a reflection of the relative strength of the kinetic energy to Coulomb attraction increasing for the hard-wall case over the parabolic potential. In other words, even though we use nominally the same width ($= 2\sqrt{\hbar/\mu\omega}$ for the parabolic po-
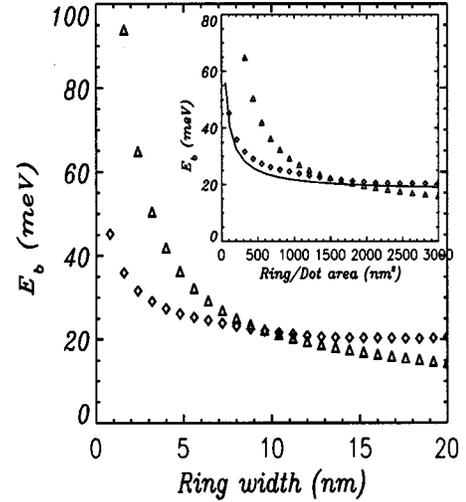

FIG. 1. Quantum ring heavy-hole exciton binding energies for parabolic (triangles) and hard-wall (diamonds) confinement potential, as function of the ring width. Inset: Same exciton binding energies as a function of the area for quantum rings (triangles and diamonds traces), and quantum dot (solid line) with the same area.

tential and $2L$ for the hard wall), the parabolic potential solutions are effectively less confined due to the finite amplitude ''leaking'' out of the ring. It is also interesting to emphasize that for smaller ring widths, the resulting wave functions are increasingly elongated *along* the ring, and this is more the case for the hard-wall confinement. In contrast, the exciton binding energy appears larger for the hard-wall confinement, for widths larger than a_B^{2D}, due to the known poor convergence of the parabolic basis used (e.g., see a detailed discussion of this problem in Ref. 20). In the range of widths shown, both approaches have converged numerically to within a few percent everywhere, and at least an order of magnitude better for the lower two-thirds of the range).

The inset in Fig. 1 compares the ring results with those of a quantum dot (with parabolic confinement[20]) with equal confinement *area* (solid line). For wider ring systems all energies are basically equal, as the confinement potential is a weak perturbation to the Coulomb interaction between carriers, as one would expect, be it ring or dot. On the other hand, the exciton binding energies in the narrower rings are larger than in the dot case with the same area, a reflection of the anisotropic confinement in the ring: For the narrow rings, the circular symmetry of the 2D free exciton (either free or in the dot) is strongly affected, and the exciton elongates along the ring, as described previously. We should mention that the *curvature* of the ring has not much effect on the ground state or binding energies for the dimensions considered here, similar to the experimental values.

To indicate the role of the Coulomb potential on the exciton characteristics, Fig. 2 shows the ground state energy of the electron–hole pair in the parabolic-confinement ring with (triangles) and without (diamond) Coulomb interaction. For a smaller ring width, the Coulomb contribution clearly increases, but not as fast as the confinement energy itself. The inset shows the electron–hole separation versus the ring width. For small width, the confinement energy is clearly
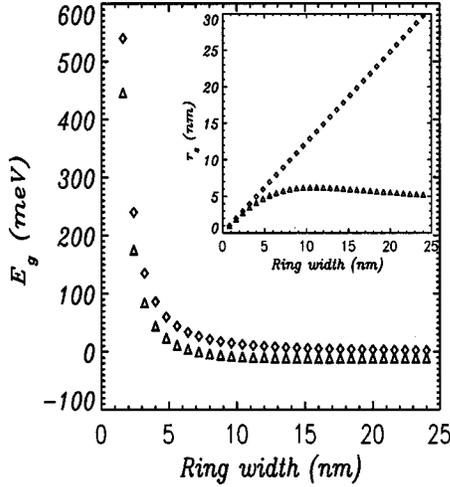
FIG. 2. Heavy-hole exciton ground state energy for parabolic confinement, as a function of the ring width. Inset: Electron–hole separation vs ring width. Triangle and diamond points are results for both with and without electron–hole Coulomb interaction, respectively.

dominant in determining the electron–hole separation, rather than the Coulomb interaction term. For widths larger than ≈ 4 nm, however, the electron–hole separation depends mostly on the Coulomb interaction term. Notice, however, that the rapid vanishing of r_s for thin rings is somewhat of a biasing artifact produced by the basis functions we use in the parabolic ring. The necessary truncation of the basis appears to favor a circularly symmetric exciton, clearly not the case in very thin rings.

Figure 3 shows the exciton binding energy and electron–hole separation versus the external magnetic field, for several ring widths, for a ring with middle radius $r_0 = 20$ nm. One can see that for larger values of the confinement energy (i.e., smaller widths), the effect of the magnetic fields is weaker, yielding the slowly changing curves at the top. However, for the larger widths, the dependence of the exciton binding energy on magnetic fields increases, resulting in the strong enhancement of the binding energies and decreasing exciton sizes with field. Notice that for larger values of the field, the exciton binding energy changes little as function of the ring width, showing that the confinement provided by the magnetic field is dominant. This is to be expected, given that the magnetic length, $l_c = \sqrt{\hbar/\mu\omega_c}$ overtakes the exciton radius at about 18 T.

For the radius of the ring in this figure, $r_0 = 20$ nm, one expects ABE oscillations with a periodicity given by multiples of $B\pi r_0^2/\phi_0$ (where $\phi_0 = hc/e = 4.14 \times 10^{-7}$ G cm^2 is the flux quantum), or a period $\Delta B \approx 3.3$ T. We find no appreciable evidence of ABE oscillations in either the binding energy or the exciton effective size, r_s. This result suggests that it is likely that ABE exciton oscillations will not be seen in measurements of the ground state properties of the exciton.

Since there is a prediction that the ABE oscillations are to be found much more easily in the case of excited states,[11] we have also looked for them in the linear optical susceptibility
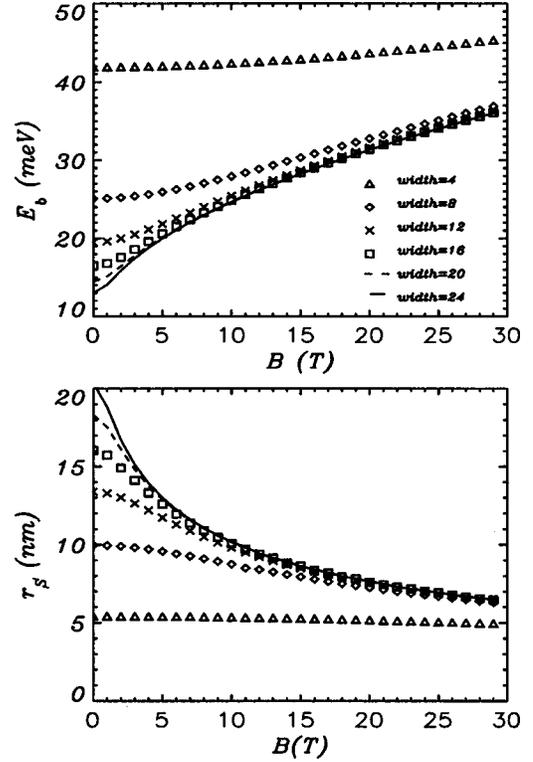

FIG. 3. Upper panel: Heavy-hole exciton binding energy as a function of magnetic field for rings with $r_0 = 20$ nm. Bottom panel: Electron–hole separation as a function of magnetic field for the same rings. Different symbols, as shown, indicate parabolic ring width for heavy hole in nm.

of a quantum ring. Figure 4 shows a typical result for different values of the magnetic field. This curve represents all the possible transitions of this excitonic state which would be measurable via photoluminescence excitation measurements (PLE; while the first peak gives the PL response). The higher peaks, starting from the one at lowest energy, correspond to electron–hole excitations involving the heavy-hole exciton ground state and various center-of-mass replicas (i.e., increasing excitations of the center-of-mass degree of freedom, without altering the ground state of the relative coordinate).
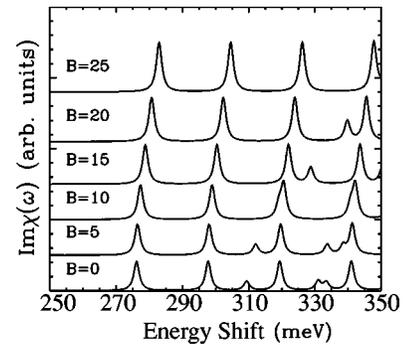

FIG. 4. Linear optical susceptibility χ for parabolic quantum ring with confinement energy $\hbar\omega_0 = 10.8$ meV (exciton *width* $= 21$ nm) for magnetic fields ranging from 0 to 25 T. Radius of the ring is 24 nm. Energy blueshift includes both in-plane and z-axis confinement (z-axis well width$= 3$ nm).

On the other hand, the smaller amplitude peaks (at shift ≈ 310, 330 meV for $B=0$), correspond to *internal* excited states of the exciton (its relative coordinate). These peaks are strongly upshifted with magnetic field, as the diamagnetic effect for each charge carrier pushes all relative energies upwards as well, and clearly these excited states shift even faster. This behavior is qualitatively similar to the excitons in a quantum dot.[21] We should also point out that in addition to the overall upward shift due to the diamagnetic effect, the χ traces show no discernible superimposed ABE oscillations with magnetic field in any of the excited states. It would appear that the finite width of the system suppresses the ABE predicted for the 1D ring.

We should also mention that higher excited states are likely to exhibit the ABE effect, as per earlier work.[11] However, the parabolic or hard-wall confinement models used in this calculation lose validity, since non-parabolic corrections to the effective mass Hamiltonian, as well as finite confinement potential effects would become more important. Consequently, a quantitative estimate of the anticipated ABE effects for high-lying states is less reliable, and more subject to specific values of parameters. A weaker confinement might also enhance ABE, although experiments in that regime would be harder to identify and characterize uniquely.

IV. CONCLUSIONS

We have shown that magnetic field has strong effects on excitons in a quantum ring, for both parabolic and hard-wall confinement potentials. Using direct matrix diagonalization techniques, we have shown that at least for rings currently realizable, the excitons behave to a great extent as those in quantum dots of similar dimensions: There are strong diamagnetic shifts and restructuring of the overall excitation manifold, large shifts of internal excitations, and reduction of the effective exciton size. On the other hand, the predicted ABE oscillations in the various physical characteristics (including binding energy and oscillator strength of transitions) of 1D excitons, are not found in this more realistic calculation. Although we anticipated that the predicted ABE effects would be much weaker (due to the finite transverse size of the rings and ring radii larger than the exciton size), we have not been able to detect any oscillation ''remnant,'' in any of the features we analyzed.

This negative result is due to either of two reasons, we surmise: one, the result of exponentially small ABE amplitudes (given the somewhat larger ring radii).[11] More likely, perhaps, this is the result of destructive interference of relatively many transverse eigenstates (mixed by the Coulomb interaction), each with its own different phase and amplitude. Notice that this is quite different for multiple-electron states in the ring, as predicted by theory, and recently seen in experiment.[5] The difference in result from the case of only electrons in the ring to that of an exciton, indicates the predicted fragility of the effect, since in this system the net charge (and then coupling to the magnetic vector potential) is zero. In fact, the delicate nature of the ABE suggests that smaller and *narrower* rings are needed in experiment, which may make for more one-dimensional-like excitons. Following our above-given discussion, one could also expect ABE oscillations to be more important for higher-excited states, even if more challenging in experiments. Perhaps one could also think of a technique that explores *differences*, and therefore is able to couple only to a modulation of the hole population, for example, as a sensitive way to access these coherent ABE oscillations for low-lying states.

Note added. Since submission, we have become aware of a preprint where calculations for rings suggest a positive result for the appearance of ABE oscillations [H. Hu, J.-L. Zhu, D.-J. Li, and J.-J. Xiong, cond-mat/0010310 (unpublished)]. Our results here are not in contradiction with those, we believe, since their somewhat unrealistically narrow rings enhance the ABE oscillations, as we discuss. Those results in fact validate our suspicion that narrower rings, if possible, are needed for these effects to be seen.

ACKNOWLEDGMENTS

APPENDIX

The matrix elements of H'_{rel}, including the Coulomb interaction term, can be calculated by using the parabolic ring basis,

$$\langle N'l'_{CM}n'l'|H'_{rel}|Nl_{CM}nl\rangle = -\delta_{N',N}\delta_{l'_{CM},l_{CM}}\delta_{l',l}\left\{ \sqrt{\frac{n!n'!}{(n+|l|)!(n'+|l'|)!}}\times\sum_{k=0}^{n}\sum_{j=0}^{n'}\frac{(n+|l|)!(n'+|l'|)!}{(k+|l|)!(j+|l'|)!} \right.$$

$$\left. \times(-1)^{k+j}\frac{1}{k!(n-k)!j!(n'-j)!}\times\frac{e^2}{\epsilon}\beta\Gamma\left(|l|+k+j+\frac{1}{2}\right)+\frac{eB\hbar l}{2\mu'c}\delta_{n',n} \right\}. \tag{A1}$$

The matrix elements of the mixing terms between the center of mass and relative coordinates, in the limit $r\ll R$, are of the form

$$\langle N'l'_{CM}n'l'|H_{mix}|Nl_{CM}nl\rangle = \sqrt{\frac{n!n'!}{(n+|l|)!(n'+|l'|)!}}2\alpha^2\sqrt{\frac{N!N'!}{(N+|l_{CM}|)!(N'+|l'_{CM}|)!}}$$

$$\times\sum_{k=0}^{n}\sum_{j=0}^{n'}\frac{(n+|l|)!(n'+|l'|)!}{(k+|l|)!(j+|l'|)!}(-1)^{k+j}\frac{1}{k!(n-k)!j!(n'-j)!}$$

$$\times\sum_{K=0}^{N}\sum_{J=0}^{N'}\frac{(N+|l_{CM}|)!(N'+|l'_{CM}|)!}{(K+|l_{CM}|)!(J+|l'_{CM}|)!}(-1)^{K+J}\frac{1}{K!(N-K)!J!(N'-J)!}$$

$$\times\left[\frac{eB\hbar}{Mc\beta}\Gamma\left(\frac{2j+2k+|l|+|l'|+3}{2}\right)\left\{\left[-\frac{1}{4\alpha}\Gamma\left(\frac{2J+2K+|l_{CM}|+|l'_{CM}|+3}{2}\right)\right.\right.\right.$$

$$+\frac{1}{4\alpha}(2K+|l_{CM}|)\Gamma\left(\frac{2J+2K+|l_{CM}|+|l'_{CM}|+1}{2}\right)-\frac{r_0}{4}\Gamma\left(\frac{2J+2K+|l_{CM}|+|l'_{CM}|+2}{2}\right)$$

$$+\frac{r_o}{4}(2K+|l_{CM}|)\times\Gamma\left(\frac{2J+2K+|l_{CM}|+|l'_{CM}|}{2}\right)\right][\delta_{l,l'+1}\delta_{l_{CM},l'_{CM}-1}-\delta_{l,l'-1}\delta_{l_{CM},l'_{CM}+1}]$$

$$-[\delta_{l,l'+1}\delta_{l_{CM},l'_{CM}-1}+\delta_{l,l'-1}\delta_{l_{CM},l'_{CM}+1}]\frac{l_{CM}}{4\alpha}\Gamma\left(\frac{2J+2K+|l_{CM}|+|l'_{CM}|+1}{2}\right)\right\}$$

$$-\frac{\mu\omega_0^2r_o}{4\alpha\beta^2}\delta_{l,l'}\delta_{l_{CM},l'_{CM}}(|l|+k+j)!\left\{\Gamma\left(|l_{CM}|+K+J+\frac{1}{2}\right)\right.$$

$$\left.\left.-e^{-\alpha^2r_0^2}\sum_{jj=0}^{\infty}\frac{\left(|l_{CM}|+K+J-\frac{1}{2}\right)!}{\left(|l_{CM}|+K+J+\frac{1}{2}+jj\right)!}(\alpha^2r_o^2)^{|l_{CM}|+K+J+\frac{1}{2}+jj}\right\}\right]. \tag{A2}$$

Coulomb interaction in hard-wall confinement,[18,21] is given by

$$H_{e-h}(\mathbf{q}) = -\frac{e^2}{\epsilon}(2\pi)^2\int\frac{1\mathbf{r}_{e-h}-i\mathbf{q}\cdot\mathbf{r}_{e-h}}{e}d\mathbf{r}_{e-h} = -2\pi\frac{e^2}{\epsilon}\frac{1}{q}, \tag{A3}$$

and

$$\Psi_e(\mathbf{r}_e) = \frac{1}{(2\pi)^2}\int\phi_e(\mathbf{q})e^{-i\mathbf{q}\cdot\mathbf{r}_e}d\mathbf{q}. \tag{A4}$$

The Coulomb interaction matrix elements,

$$\langle n'_el'_en'_hl'_h|H_{e-h}|n_el_en_hl_h\rangle = \int\Psi'_e(\mathbf{r}_e)\Psi'_h(\mathbf{r}_h)H_{e-h}(\mathbf{r}_{e-h})\Psi_e(\mathbf{r}_e)\Psi_h(\mathbf{r}_h)d\mathbf{r}_ed\mathbf{r}_h, \tag{A5}$$

are then rewritten as

$$\langle n'_el'_en'_hl'_h|H_{e-h}|n_el_en_hl_h\rangle = \frac{1}{(2\pi)^6}\int\phi'_e(\mathbf{q}_e)\phi'_h(\mathbf{q}_h)H_{e-h}(\mathbf{q})\phi_e(\mathbf{q}_e-\mathbf{q})\phi_h(\mathbf{q}_h+\mathbf{q})d\mathbf{q}_ed\mathbf{q}_hd\mathbf{q}, \tag{A6}$$

where the Fourier transform integrals used for electron and hole wave functions, respectively, are

$$\varphi_e(\mathbf{q}) \equiv \int \phi_e'(\mathbf{q}_e)\phi_e(\mathbf{q}_e - \mathbf{q})d\mathbf{q}_e$$

$$= (2\pi)\int_a^{a+2L} \psi_e'(r_e)\psi_e(r_e)r_e dr_e \int_0^{2\pi} e^{im\phi_e}e^{-iqr_e\cos(\phi_q-\phi_e)}d\theta_e$$

$$= (2\pi)^2(i)^{-m}e^{im\phi_q}\int_a^{a+2L} \psi_e'(r_e)\psi_e(r_e)J_m(r_e q)r_e dr_e, \tag{A7}$$

where $m = l_e - l_e'$, and the definition of the Bessel function

$$J_m(qr) = \frac{1}{2\pi}\int_{-\pi}^{\pi} e^{-im\phi+iz\sin\phi}d\phi \tag{A8}$$

has been used. A similar expression for the hole wave functions gives the interaction matrix elements

$$\langle n_e'l_e'n_h'l_h'|H_{e-h}|n_e l_e n_h l_h\rangle = -\delta_{l_e+l_h,l_e'+l_h'}\frac{e^2}{\epsilon}\int_a^{a+2L}$$

$$\times \psi_e'(r_e)\psi_e(r_e)r_e dr_e \int_a^{a+2L} \psi_h'(r_h)\psi_h(r_h)r_h dr_h$$

$$\times \int_0^{\infty} J_{|m|}(r_e q)J_{|m|}(r_h q)dq. \tag{A9}$$

In order to evaluate the integrals in Eq. (A9), we use

$$\int_0^{\infty} J_{|m|}(r_e q)J_{|m|}(r_h q)dq = \frac{r_<^{|m|}}{r_>^{|m|+1}}\frac{\Gamma\left(|m|+\frac{1}{2}\right)}{\Gamma(|m|+1)\Gamma\left(\frac{1}{2}\right)}F\left(m+\frac{1}{2},\frac{1}{2};|m|+1;\left(\frac{r_<}{r_>}\right)^2\right), \tag{A10}$$

where $r_>(r_<)$ is the larger (smaller) of r_e and r_h, and F is a hypergeometric function.[26] Inserting Eq. (A10) into Eq. (A9), the interaction matrix elements can be written as

$$\langle n_e'l_e'n_h'l_h'|H_{e-h}|n_e l_e n_h l_h\rangle = -\delta_{l_e+l_h,l_e'+l_h'}\frac{e^2}{\epsilon}\frac{\Gamma\left(|m|+\frac{1}{2}\right)}{\Gamma(|m|+1)\Gamma\left(\frac{1}{2}\right)}\times\left\{\int_a^{a+2L}\psi_e'(r_e)\psi_e(r_e)\frac{1}{r_e^{|m|}}dr_e\int_a^{r_e}\psi_h'(r_h)\psi_h(r_h)r_h^{|m|+1}\right.$$

$$\times F\left(|m|+\frac{1}{2},\frac{1}{2};|m|+1;\left(\frac{r_h}{r_e}\right)^2\right)dr_h + \int_a^{a+2L}\psi_h'(r_h)\psi_h(r_h)\frac{1}{r_h^{|m|}}dr_h\int_a^{r_h}\psi_e'(r_e)\psi_e(r_e)r_e^{|m|+1}$$

$$\left.\times F\left(|m|+\frac{1}{2},\frac{1}{2};|m|+1;\left(\frac{r_e}{r_h}\right)^2\right)dr_e\right\}. \tag{A11}$$

This greatly simplified expression for the interaction matrix elements is easily evaluated numerically. The total Hamiltonian matrix is diagonalized numerically, providing all the eigenvalues and eigenfunctions. To improve numerical convergence, we use the transformation of hypergeometric functions given by

$$F\left(|m|+\frac{1}{2},\frac{1}{2};|m|+1;z\right) = \frac{\Gamma(|m|+1)}{\Gamma\left(|m|+\frac{1}{2}\right)\Gamma\left(\frac{1}{2}\right)}\sum_{n=0}^{\infty}\frac{\left(|m|+\frac{1}{2}\right)_n\left(\frac{1}{2}\right)_n}{n!^2}$$

$$\times\left\{2\psi(n+1)-\psi\left(|m|+n+\frac{1}{2}\right)-\psi\left(n+\frac{1}{2}\right)-\ln(1-z)\right\}(1-z)^n, \tag{A12}$$

where ψ is the digamma function.[27]

The matrix elements dependent on magnetic fields are given by

$$\langle n'_e l'_e n'_h l'_h | H_B | n_e l_e n_h l_h \rangle = \delta_{l'_e,l_e} \delta_{l'_h,l_h} \Bigg\{ \left(\frac{l_h}{m_h} - \frac{l_e}{m_e} \right) \frac{\hbar e B}{2c} \int_a^{a+2L} \psi'_e(r_e)\psi_e(r_e)r_e dr_e \int_a^{a+2L} \psi'_h(r_h)\psi_h(r_h)r_h dr_h$$

$$+ \frac{e^2 B^2}{8m_e c^2} \int_a^{a+2L} \psi'_h(r_h)\psi_h(r_h)r_h dr_h \int_a^{a+2L} \psi'_e(r_e)\psi_e(r_e)r_e^3 \, dr_e$$

$$+ \frac{e^2 B^2}{8m_h c^2} \int_a^{a+2L} \psi'_e(r_e)\psi_e(r_e)r_e dr_e \int_a^{a+2L} \psi'_h(r_h)\psi_h(r_h)r_h^3 \, dr_h \Bigg\}. \tag{A13}$$

The size of the exciton is here given by

$$r_s^2 = \langle \Psi | r^2 | \Psi \rangle = \sum_{n_e n_h l_e l_h n'_e n'_h l'_e l'_h} a'_{n'_e n'_h l'_e l'_h} a_{n_e n_h l_e l_h} \Bigg\{ \delta_{l'_e,l_e}\delta_{l'_h,l_h}\Bigg(\int_a^{a+2L} \psi'_h(r_h)\psi_h(r_h)r_h dr_h \int_a^{a+2L} \psi'_e(r_e)\psi_e(r_e)r_e^3 \, dr_e$$

$$+ \int_a^{a+2L} \psi'_e(r_e)\psi_e(r_e)r_e dr_e \int_a^{a+2L} \psi'_h(r_h)\psi_h(r_h)r_h^3 dr_h \Bigg) - \delta_{l'_e+l'_h,l_e+l_h}\delta_{l'_e+1,l_e} \int_a^{a+2L} \psi'_e(r_e)\psi_e(r_e)r_e^2 \, dr_e$$

$$\times \int_a^{a+2L} \psi'_h(r_h)\psi_h(r_h)r_h^2 \, dr_h \Bigg\}. \tag{A14}$$

[1] See, for example, Proceedings of the International Conference on Semiconductor Quantum Dots, QD2000, Munich, Germany, [Phys. Status Solidi (to be published)].

[2] S. Lee, J.C. Kim, H. Rho, C.S. Kim, L.M. Smith, H.E. Jackson, J.K. Furdyna, and M. Dobrowolska, Phys. Rev. B **61**, R2405 (2000).

[3] E. Menendez-Propin, C. Trallero-Giner, and S.E. Ulloa, Phys. Rev. B **60**, 16747 (1999).

[4] M. Bayer, O. Stern, P. Hawrylak, S. Fafard, and A. Forschel, Nature (London) **405**, 923 (2000).

[5] A. Lorke, R.J. Luyken, A.O. Govorov, J.P. Kotthaus, J.M. Garcia, and P.M. Petroff, Phys. Rev. Lett. **84**, 2223 (2000).

[6] J.M. Garcia, G. Medeiros-Ribeiro, K. Schmidt, T. Ngo, J.L. Feng, A. Lorke, J. Kotthaus, and P.M. Petroff, Appl. Phys. Lett. **71**, 2014 (1997).

[7] See, for example, M. Büttiker, Y. Imry, and R. Landauer, Phys. Lett. **96A**, 365 (1983); L.P. Lévy, G. Dolan, J. Dunsmuir, and H. Bouchiat, Phys. Rev. Lett. **64**, 2074 (1990); V. Chandrasekhar, R.A. Webb, M.J. Brady, M.B. Ketchen, W.J. Gallagher, and A. Kleinsasse, *ibid.* **67**, 3578 (1991); D. Mailly, C. Chapelier, and A. Benoit, *ibid.* **70**, 2020 (1993).

[8] T. Chakraborty and P. Pietilainen, Phys. Rev. B **50**, 8460 (1994); **52**, 1932 (1995).

[9] I. Krive and A.A. Krokhin, Phys. Lett. A **186**, 162 (1994).

[10] A. Chaplik, JETP Lett. **62**, 900 (1995).

[11] R.A. Römer and M.E. Raikh, cond-mat/9906314 (unpublished).

[12] A. Gracia-Cristobal and C. Trallero-Giner (unpublished).

[13] R.J. Warburton, C. Schäflein, D. Haft, F. Bickel, A. Lorke, K. Karrai, J.M. Garcia, W. Schoenfeld, and P.M. Petroff, Nature (London) **405**, 926 (2000).

[14] F. Findis, A. Zrenner, G. Böhm, and G. Abstreiter, Solid State Commun. **114**, 227 (2000).

[15] J.C. Maan, G. Belle, A. Fasolino, M. Altarelli, and K. Ploog, Phys. Rev. B **30**, 2253 (1984).

[16] J. Cen and K.K. Bajaj, Phys. Rev. B **46**, 15280 (1992).

[17] M. Kohl, D. Heitmann, P. Grambow, and K. Ploog, Phys. Rev. Lett. **63**, 2124 (1989).

[18] V. Halonen, T. Chakraborty, and P. Pietiläinen, Phys. Rev. B **45**, 5980 (1992).

[19] L. Jacak, P. Hawrylak, and A. Wojs, *Quantum Dots* (Springer, Berlin, 1998), and references therein.

[20] J. Song and S.E. Ulloa, Phys. Rev. B **52**, 9015 (1995).

[21] P. Pereyra and S.E. Ulloa, Phys. Rev. B **61**, 2128 (2000).

[22] K.L. Janssens, F.M. Peeters, and V.A. Schweigert, cond-mat/0002405 (unpublished).

[23] See, for example, L.W. Wang, A.J. Williamson, A. Zunger, H. Jiang, and J. Singh, Appl. Phys. Lett. **76**, 339 (2000), and references therein.

[24] *Handbook of Mathematical Functions*, edited by M. Abramowitz and I. A. Stegun (Dover, New York, 1972), P. 374.

[25] C. Hermann and C. Weisbuch, Phys. Rev. B **15**, 823 (1977).

[26] *Table of Integrals, Series and Products*, edited by I. S. Gradshteyn and I. M. Ryzhik (Academic, San Diego, 1994), P. 693.

[27] *Special Functions & Their Applications*, edited by N. N. Lebedev (Dover, New York, 1972), p. 6.